Journal of Magnetic Resonance Open 10-11 (2022) 100039

Contents lists available at ScienceDirect

Journal of Magnetic Resonance Open

journal homepage: www.sciencedirect.com/journal/journal-of-magnetic-resonance-open

Research Article

CW-EPR spectra of P1 centers in HPHT diamond in the vicinity of Rabi resonance: possible standard for B_1 evaluation in EPR and DNP enhanced NMR spectroscopies

B. Rakvin *, D. Carić, M. Kveder

Ruđer Bošković Institute, Division of Physical Chemistry, Bijenička 54, Zagreb, Croatia.

ARTICLE INFO

Keywords:
P1 centers in diamond
EPR
DNP
Electron spin relaxation
Modulation sidebands

ABSTRACT

Synthetic commercial type-IIa diamond crystal containing low concentration of P1 (N_s^0) centers ([N_s^0] <1ppm) was examined as a possible calibration standard for evaluating microwave magnetic field intensity (B_1) in the spectrometer cavity. The reliability of this standard was experimentally and theoretically tested by employing two different types of microwave cavities with different distributions of B_1 values. The procedure relies on the ordinary continuous wave electron paramagnetic resonance (CW-EPR) with magnetic field modulation ($\omega_{rf}/2\pi =$ 100 kHz) applied under the regime of the microwave power (P_{MW}) saturation of the out-of-phase first harmonic signal. The power saturation procedure for $P_{MW} \sim B_1^{1/2}$ was analyzed with respect to the change of spectral lineshape when Rabi frequency ($\omega_1 = \gamma B_1$, γ is the electron gyromagnetic ratio) approaches to ω_{rf}. The phenomenon of the inversion of sideband lines while passing the Rabi resonance condition ($\omega_1 = \omega_{rf}$) was analyzed. In specific, from the simulation of the experimental lineshapes in the close vicinity of Rabi resonance ($\omega_1 \approx \omega_{rf}$) the corresponding B_1 can be assigned. For the chosen diamond crystal low value of $B_1 \approx 3.6$ μT at Rabi resonance was determined what makes it a convenient standard for DNP enhanced NMR spectroscopy which requires relatively small B_1.

1. Introduction

In a continuous wave electron paramagnetic resonance (CW-EPR) spectroscopy the intensity of microwave (MW) magnetic field (B_1) traditionally can be determined by applying several methods [1–8]. One approach is based on employing perturbing metal sphere [1, 2] in the microwave cavity while other methods are related to the MW power (P_{MW}) saturation of the signal from the sample with known spin-spin (T_2) and spin-lattice (T_1) relaxation times. For the later techniques it is important to note that one should choose as a standard the sample with long relaxation times. These long relaxations are required to assure that the power saturation curve (signal intensity versus $P_{MW} \sim B_1^{1/2}$) shows a maximum in the available power range. It is expected that B_1 involved in the non-resonant structures, typically used for DNP-enhanced NMR, is smaller than B_1 employed in X-band CW-EPR and consequently the calibration sample for DNP should be characterized with longer relaxation times. Recently [9], commercial high pressure high temperature (HPHT) diamond containing concentration of P1 centers [N_s^0] ~30-200 ppm was proposed as a secondary standard for calibration of electron B_1 field in DNP-enhanced NMR as well as in CW-EPR. The saturation curve in CW-EPR was employed to determine T_1T_2 product of P1 centers. In addition, these relaxation times were separately evaluated by pulse measurements at X-band MW frequency. For the central peak of the P1 center the expected maximum of saturation curve was obtained at $B_1 \approx$ 5 μT. The distribution of relaxation times was detected due to inhomogeneity of the saturation peak. Thus, the quantitative calibration of B_1 required taking into account the combination of saturation curves [9]. The origin of different relaxation times was related to electron-electron spin diffusion mechanism and electron-electron dipolar coupling which contribute to the line broadening.

However, power saturation methods can be also discriminated regarding the intensity of modulation radio frequency (RF) magnetic field ($B_2 = \omega_2/\gamma$, γ denoting the electron gyromagnetic ratio) with respect to linewidth of the monitored signal (Lorentzian type with full

; DNP, dynamic nuclear polarization; EPR, electron paramagnetic resonance.

* Corresponding author.
E-mail address: rakvin@irb.hr (B. Rakvin).

https://doi.org/10.1016/j.jmro.2022.100039
Received 19 November 2021; Received in revised form 13 January 2022; Accepted 23 January 2022
Available online 24 January 2022

width at half height (FWHH), $\delta = 1/\pi T_2$). Typically, for standard modulation frequency of $\omega_{rf}/2\pi = 100$ kHz a comparable values of $\omega_2 / 2\pi \sim \delta$ have been employed [3–6] to obtain optimal signal to noise ratio of detected signal. However, in the case when $\omega_{rf}/2\pi > \delta$ the CW-EPR signal exhibits modulation sideband spectrum (MS) with $\omega_{rf}/2\pi$ splitting between the detected signals. The obtained MS spectrum can be also used for determination of B_1 [7, 8] and this approach was undertaken in here presented investigation using commercial HPHT diamond crystal with significantly lower concentration ($[N_s^0] <1$ppm) of P1 centers. This sample was chosen in order to reduce line broadening contributions, as well as to minimize possible distribution of relaxation times, and hence achieve increased T_2 relaxation time. For B_1 estimation a simple methodology of CW-EPR signal detection including MS with the corresponding theoretical background was considered due to easier implementation in DNP instrumentation than some pulsed EPR methods which can be otherwise more straightforward. Due to significantly longer relaxation times ($T_1 \approx 2$ ms, $T_2 \approx 146$ μs) [10, 11] this crystal shows saturation peak at very low microwave field and, thus, it is not convenient for the estimation of T_1T_2 product in power saturation measurement. However, the homogeneous line of this sample is very narrow ($\delta \approx 2$ kHz) and moreover, even inhomogeneous line detected in the CW-EPR shows narrow lineshape ($\delta^I_{pp} \approx 0.16$ MHz (6 μT)). For such narrow lines, which are comparable with the applied $\omega_{rf}/2\pi = 100$ kHz, it has been reported that the homogeneous lineshape of calculated out-of-phase first harmonic signal for $T_1 = T_2 = 2$ ms shows the inversion of MS lines while passing Rabi resonance condition $\omega_1 = \omega_{rf}$ [12]. This was achieved by increasing B_1 in the standard saturation process. Here, B_1 is presented in the circular frequency form as the Rabi frequency $\omega_1 = \gamma B_1$ of the MW field.

In this paper the out-of-phase first harmonic CW-EPR spectra of P1 center in HPTH diamond crystal, which show MS effects related to inversion of sideband lines, have been experimentally detected as a function of P_{MW} and used to determine the intensity of microwave magnetic field B_1. The procedure relies on previously developed theoretical formalism for MS description at Rabi resonance [12] which was adapted to simulate the acquired data for various T_1 and T_2 relaxation times leading ultimately to the spectrum corresponding to the condition of $\omega_1 \approx \omega_{rf}$, thus, providing B_1 determination. The assigned resonance spectrum in the saturation process was correlated with the experimental spectra in order to define value of P_{MW} at which $\omega_1/2\pi = 100$ kHz and $B_1 \approx 3.6$ μT is to be expected. Since experimental spectra exhibit inhomogeneous character, two qualitative parameters ($D_{\pm 1}$, Δ_{pp}) were introduced in the spectral analysis with the aim to facilitate the assignment of the experimental spectra in the close vicinity of Rabi resonance.

2. Materials and methods

The CW-EPR experiments were performed using Bruker ELEXSYS 580 spectrometer working at X-band frequency. The spectra were recorded by employing two different microwave cavities, Bruker ER 4118X-MD5 and Rectangular cavity TE_{102} equipped with the same 200 mW source (including variable attenuation which is presented in dB below 200 mW) of microwave radiation. All CW-EPR spectra were recorded with 1024 points resolution by keeping other spectral parameters at the same values (as much as possible) in order to easier correlate detected Rabi resonance effects between various spectra.

The diamond sample used in the present study was synthetic diamond type-IIa crystal (2.46 × 2.46 × 0.95 mm^3, with polished face normal to the [100] axis) produced by Element 6. This type of crystal is transparent and characterized by low concentration of impurities ($[N_s^0]$ <1 ppm and boron concentration < 0.05 ppm. The long relaxation times for such type of crystal and presence of corresponding narrow lines were estimated previously [10, 11]. The [1,0,0] crystal axis is aligned along the Zeeman magnetic field with accuracy of experimental error ($\pm 1^o$) in the CW-EPR cavity. Thus, the expected 1:1:1 intensity of spectral lines at this orientation usually appears as triplet spectrum with non-equivalent intensities of lines (with higher intensity of central line in comparison to outer lines, (m_I=±1)) due to small misalignment of the crystal and anisotropy of ^{14}N hyperfine splitting. Although, the effect of Rabi resonance affects all three lines it is convenient to monitored this effect on the central line due to the smallest effect of uncertainty of the crystal orientation.

3. Theoretical background: out-of-phase first harmonic at Rabi resonance

Conventional CW-EPR spectrometer uses magnetic field modulation ($2\omega_2 \sin\omega_{rf}$) in order to increase signal to noise ratio of detected signal. In the case when $\omega_{rf}, 2\omega_2 > 2\pi\delta$, detected spectrum appears in the form of MS showing spectral peaks (sidebands) at each multiple of $k\omega_{rf}$, ($k = 1, 2, \ldots$.) symmetrically with respect to the center of the spectrum [13, 14]. It is important to note that the obtained sideband lines show nearly the same linewidth as the linewidth of the original line in the absence of modulation. It should be emphasized, that the properties of MS spectra detected by conventional CW-EPR at the Rabi resonance have not been studied in detail in spite of their potential to be employed for determination of B_1 value. Considering such an approach to deduce B_1 value, one substantial problem appears due to the fact that theoretical prediction of the spectrum lineshape is based on homogeneous line while usually experimentally detected lineshape exhibits inhomogeneous character.

3.1. Simulation of spectra assuming various T_1 and T_2

In the present study the lineshapes of spectra in the near vicinity of Rabi resonance were studied as a function of various relaxation times. The theoretical formalism describes a qubit with dephasing rate η and relaxation rates $\gamma_\parallel = 1/T_1$ and $\gamma_\perp = 1/T_2$ where $\gamma_\parallel = \gamma_{12} + \gamma_{21}$ and $\gamma_\perp = (\gamma_{12} + \gamma_{21} + \eta)/2$ are energetic and phase relaxation rates in the laboratory frame, respectively. The interaction with transverse MW and longitudinal RF fields is assumed [12] under the condition of "weak modulation near the Rabi resonance" ($\omega_2 \ll \omega_1 \approx \omega_{rf}$). In this regime of weak modulation near the Rabi resonance the first harmonic CW-EPR signal, V^{st}, given by Eq. (1)

$$V^{st} = A_1^{\frac{\pi}{2}} \sin\omega_{rf} t + A_1^0 \cos\omega_{rf} t. \tag{1}$$

The signal detected along with the modulation phase (A_1^0, in-phase signal) appears with lower intensity than the signal detected at π/2-out-of-phase ($A_1^{\pi/2}$, out-of-phase signal). The analytical expression for the amplitude of the first harmonic out-of-phase signal was estimated earlier [12]

$$A_1^{\pi/2} = \sigma_0 \sum_k \frac{\square_k w_k}{2\Gamma_\perp^2} \frac{J_{1-k}(a) - J_{-1-k}(a)}{1 + \frac{w_k^2}{\Gamma_\perp \Gamma_\parallel} + \frac{w_k^2}{\Gamma_\perp^2}} \tag{2}$$

with $\omega_0 = \gamma B_0$ denoting Larmor frequency, ω_{mw} is MW frequency, $\Delta = \omega_0 - \omega_{mw}$ is frequency shift while $\Omega = \sqrt{\omega_1^2 + \Delta^2}$, $\sin\theta = \omega_1/\Omega$, $\cos\theta = \Delta/\Omega$, $\Gamma_\parallel = \gamma_\parallel + (\gamma_\perp - \gamma_\parallel)\sin^2\theta$, $\Gamma_\perp = \gamma_\perp - \frac{1}{2}(\gamma_\perp - \gamma_\parallel)\sin^2\theta$, $\sigma_0 = (\gamma_{21} - \gamma_{12})\cos\theta/\Gamma_\parallel$ and the modulation index of the Bessel function of the first kind and order k, $J_k(a)$ is given by $a = 2\omega_2\cos\theta/\omega_{rf}$. The

following abbreviations are used:

$$\square_k = \Omega - k\omega_{rf} + \Delta_{BS}(k) \tag{2a}$$

$$\Delta_{BS}(k) = \frac{\omega_2^2 \sin^2\theta}{2\omega_{rf}}\left[\sum_{n\neq -k+1}\frac{1}{n+k-1}\left(J_n^2(a)+J_n(a)J_{n-2}(a)\right)+\sum_{n\neq -k-1}\frac{1}{n+k+1}\left(J_n^2(a)+J_n(a)J_{n+2}(a)\right)\right] \tag{2b}$$

$$w_k = \frac{\omega_1\omega_{rf}k}{\Delta}J_{-k}(a) \tag{2c}$$

Relations (2a-2c), can be also used for description of *k*-sideband, resonance positions, Bloch-Sigert-like shift and saturation, respectively. Calculated and experimental spectra were correlated in order to assign the best approximation for the lineshape at Rabi resonance. The expected narrow spectral linewidths for the chosen diamond crystal could be deduced from previously reported pulsed-EPR [10] and DM-EPR [11] experimental studies at room temperature. The narrowest linewidth was described by $T_1 = 2$ ms, and $T_2 = 146$ μs determined from pulsed-EPR measurements at 115 GHz [10]. The presence of such narrow lines exhibiting $\delta \approx 2$ kHz was also confirmed by DM-EPR at X-band frequencies [11]. However, both methods also indicated the presence of broader linewidth. For such low density crystal pulsed-EPR with double electron-electron resonance (DEER) method was employed to detect the linewidth exhibiting $\delta \sim 54$ kHz due to the spin-spin interactions and assigned to an effective T_2* spanning the range from 3.7- 5.9 μs [10]. The presence of the broad linewidth component with the corresponding effective correlation time $T_2^* \sim 20$ μs was also observed in the DM-EPR study [11]. Therefore, considering the above experimental evidences for the monitored crystal it became obvious that dependence of the lineshape at Rabi resonance should be investigated within the broad interval (3.7 μs-146 μs) of relaxation times. Figure 1. shows simulated out-of-phase signal near and at Rabi resonance $\omega_1 = 0.9\omega_{rf}, \omega_1 = \omega_{rf}$ and $\omega_1 = 1.1\omega_{rf}$ for the longest, $T_2 = 146$ μs and the shortest, $T_2 \sim 3.7$ μs, relaxation times. It is easy to note that the expected broad structure of lineshape for both fast and slow relaxation times qualitatively describes well the resonance position. The spectral features of the second sideband became too broad to be clearly assigned in spectrum. It can be noticed that the amplitude of the broad spectral lineshape is significantly smaller than the amplitude of the narrow one. However, the shape of the spectra in the close vicinity of the center exhibits similar behavior for all three values of ω_1 and hence one can still well assign the resonance position of broad spectrum. The consequence of this finding is very important for the feasibility of assigning Rabi resonance in the broad distribution of homogeneous linewidths. Here, significant variation in the intensity distribution is observed while the shape distribution of the spectral components shows similar behavior in the near vicinity of the center. In addition, spectral simulation can be performed to examine how the changing of the effective T_1 values while keeping T_2 constant affects the spectral lineshape. The spectra in the vicinity of Rabi resonance ($\omega_1 = 0.9\omega_{rf}, \omega_1 = \omega_{rf}$ and $\omega_1 = 1.1\omega_{rf}$) for T_1 values changed in the range of two orders of magnitude are shown in Fig. 2. All the spectra simulated with shorter T_1 show minor decrease in the intensity and additional narrowing in comparison to the spectra simulated with longer T_1. Thus, it can be concluded that distribution of $T_1$and T_2 produces different impacts on lineshape features at Rabi resonance.

4. Detection of first harmonic out-of-phase absorption signal of P1 center in diamond

P1, (N_s^0) center is known as the most common paramagnetic impurity in natural and as-grown CVD diamonds and it was studied by

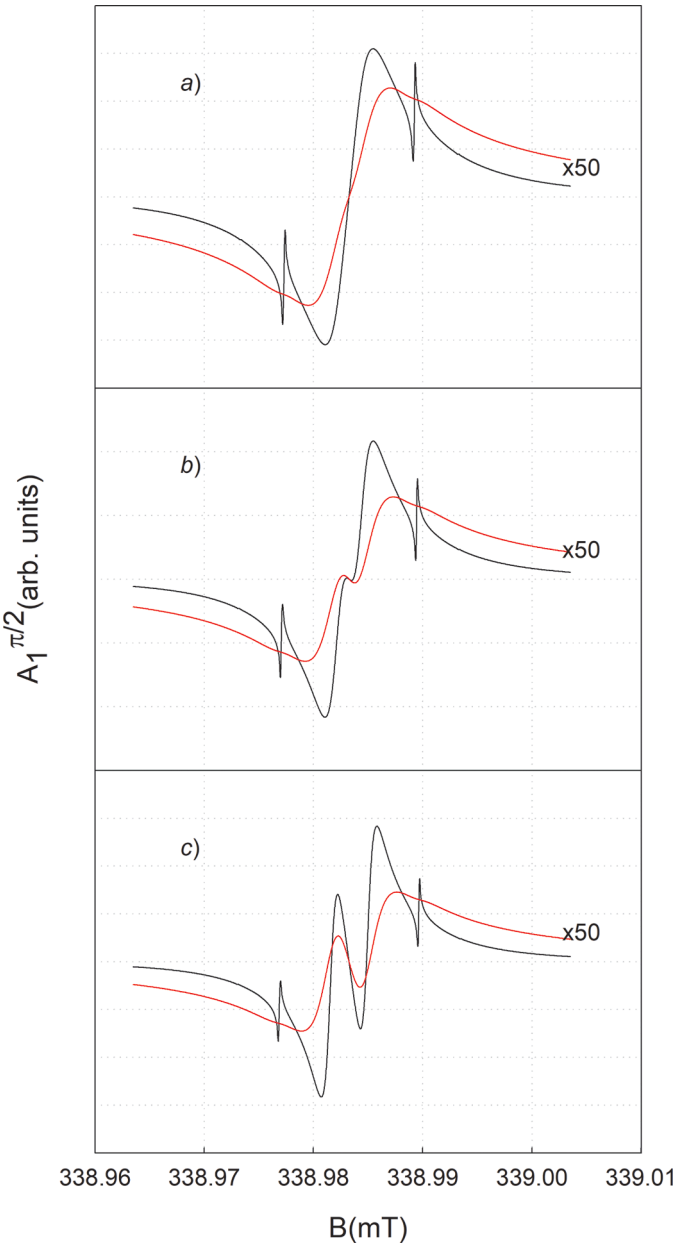

Figure 1. The first-harmonic out-of-phase absorption EPR signal calculated from Eq.2 for $T_1 = 2$ ms and two different values of T_2 (146 μs, black spectrum and 3.7 μs, red spectrum) as a function of ω_1. a) $\omega_1 = 0.9\omega_{rf}$, b) $\omega_1 = \omega_{rf}$ and c) $\omega_1 = 1.1\omega_{rf}$. All the spectra for shorter relaxation time exhibit significantly smaller intensity than the spectra for longer relaxation time.

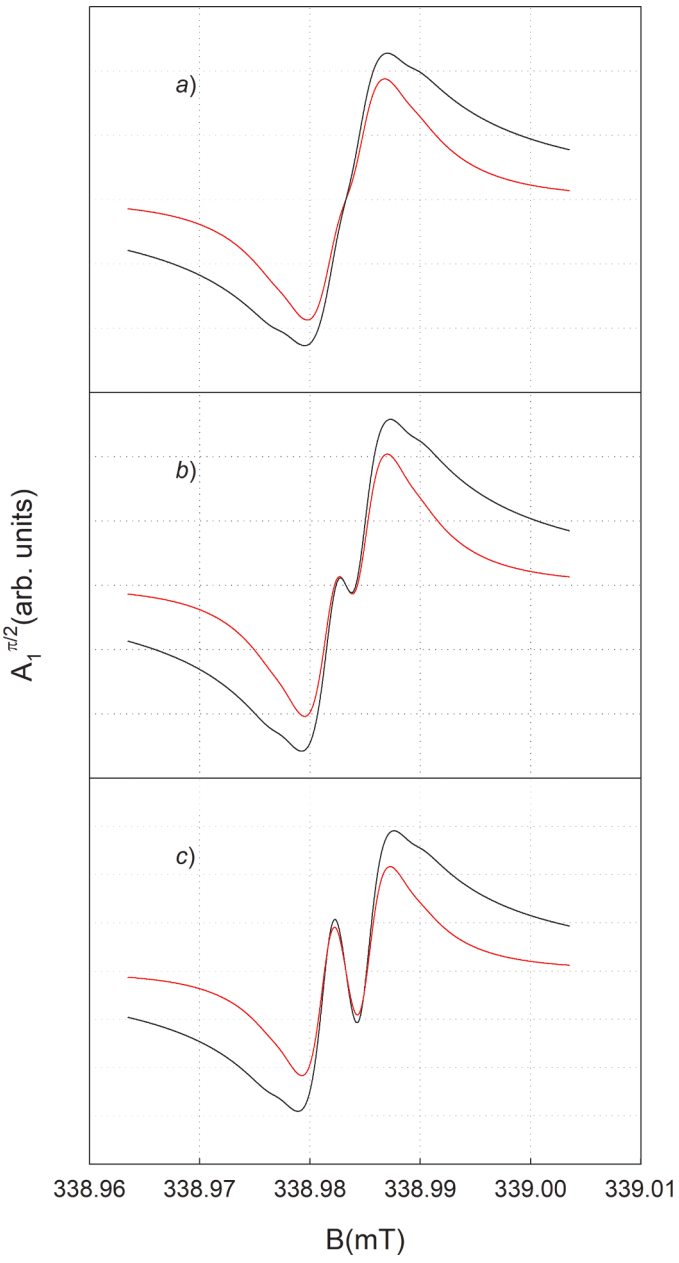

Figure 2. The first-harmonic out-of-phase absorption EPR signal calculated from Eq.2 for $T_2 = 3.7$ μs and two different values of T_1 (2 ms which corresponds to black spectrum and 20 μs which corresponds to red spectrum) as function of ω_1. a) $\omega_1 = 0.9\omega_{rf}$, b) $\omega_1 = \omega_{rf}$ and c) $\omega_1 = 1.1\omega_{rf}$. Other parameters are the same as in Fig. 1.

various EPR methods [15–18]. It exhibits $S = 1/2$, $I = 1$ (from ^{14}N nucleus) and C_{3v} symmetry. This system can be described by four independent sites in a diamond lattice. When B_0 is aligned parallel to [100] crystallographic direction (perpendicular to the face of the type-IIa crystal), nitrogen-carbon anti-bonding orbitals (localization of unpaired electron) of all four sites make the same angle with B_0 and all four sites give identical spectrum. This spectrum is characterized with a dominant triplet line splitting due to the hyperfine interaction with the spin of the nitrogen nucleus (Fig. 3). The intensities of the triplet lines indicate small deviation from the expected 1:1:1 ratio showing larger intensity for the central line in comparison to the outer lines. It was estimated that this deviation is caused by uncertainty in the crystal orientation (within experimental error of $\pm 1^o$ between [1,0,0] crystal axis and direction of magnetic field) since additional spectral lines from

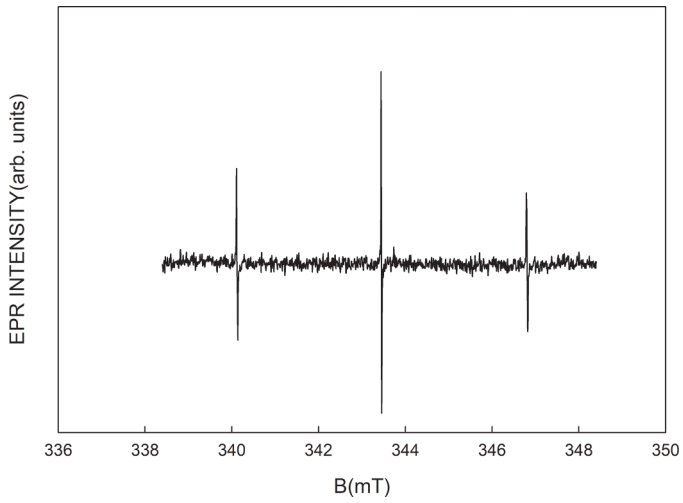

Figure 3. CW-EPR spectrum of P1 center when B_0 is aligned parallel to [100] crystal direction detected at the first harmonic of modulation frequency. The following parameters were applied: $\omega_{rf}/2\pi = 100$ kHz, $\omega_2/2\pi = 81$ kHz and $P_{MW} = 30$ dB.

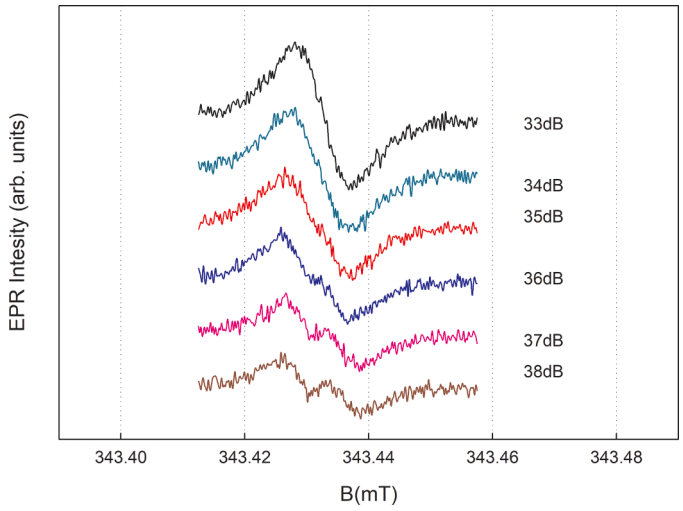

Figure 4. CW-EPR spectra of P1 spectrum in the near vicinity of the central line as a function of MW power. The recording parameters were the same as in Fig. 3 except for the applied $\omega_2/2\pi = 27$ kHz.

the other centers remained undetectable at employed low MW power. Each line exhibits an additional inhomogeneous broadening due to the ^{13}C hyperfine splitting, dipole-dipole interaction with other paramagnetic centers in the vicinity of P1 and the presence of certain level of saturation broadening due to the long relaxation times. In order to detect undistorted spectra of this sample a low value of ω_{rf}, ω_2 and ω_1 recording parameters in CW-EPR are required. However, this choice of parameters cause signal to noise ratio (S/N) in the CW spectra to be very low and insufficient for detecting the line intensity. For example, the special type-IIa synthetic diamond crystal with reduced concentration of ^{13}C isotope presents one of the narrowest peak-to-peak linewidths of P1 center detected at the first harmonic ($\delta^I_{pp} = 4$ μT) of CW-EPR at low values of recording parameters (modulation frequency 25 kHz, modulation amplitude 1 μT and microwave power 60 μW) [18]. It was also noted that by applying the rapid passage (RP) RP-EPR technique [19, 20] one can improve S/N in detecting the low concentration of P1 centers. The amount of improvement of P1 center detection was evaluated and discussed in the study comparing CW-EPR, pulsed-EPR and

RP-EPR methods [21]. It is important to mention that although RP-EPR improves *S/N* in detecting P1 center exhibiting $\delta_{pp}^{I} = 4.5$ μT, its Lorentzian line shape is much broader than the expected spin-packet linewidth of cca. 0.04 μT calculated for T_2=146 μs. In order to investigate the effect of modulation sidebands on the P1 spectra the central line in the spectrum was closely monitored as a function of MW power as shown in Fig. 4. It can be easily noted that the obtained splitting of the central line (as well as for outer m_I=±1 lines which was also detected) lines in the spectrum depends on the intensity of applied MW power in the spectrometer cavity. The same type of behavior of the central line of diamond crystal containing low concentration of P1 centers has been observed previously by employing similar detection parameters [22]. However, the observed phenomenon was not completely explained until the MS model was applied [12].

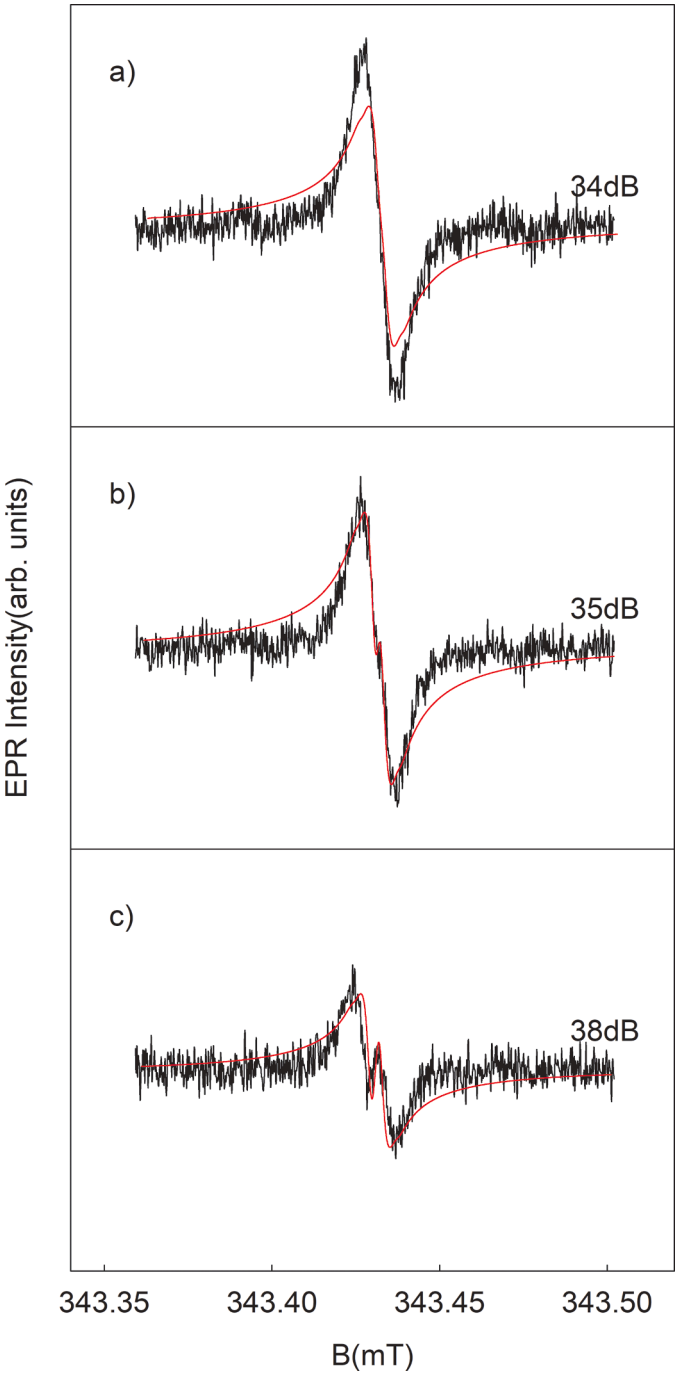

Figure 5. EPR spectra of P1 center detected as function of microwave power expressed as attenuation of MW in dB (solid black line) and corresponding simulated spectra (red line). Parameters for calculated spectra are: $T_1 = 2$ ms, $T_2 = 3.7$ μs, a) $\omega_1 = 1.1\omega_{rf}$, b) $\omega_1 = \omega_{rf}$, c) $\omega_1 = 0.9\omega_{rf}$. Besides the change of ω_1 for each spectrum all other parameters involved in the simulation were unchanged.

5. Results and discussion

5.1. Correlation between detected and calculated spectra at Rabi resonance

Following the above considerations, it is clear that spectra simulated with short $T_2 = 3.7$ μs better describe detected spectra than those simulated with long $T_2 = 146$ μs. As demonstrated in Fig. 1 the 2nd sideband contribution can be only clearly noted for longer relaxation time while for shorter relaxation time this feature cannot be clearly resolved. Thus, $T_1 = 2$ ms and $T_2 = 3.7$ μs were chosen for simulation of the experimental spectra in the vicinity of Rabi resonance as shown in Fig. 4. Correlation between simulated and experimental spectra is shown in Fig. 5 for ω_1 ($\omega_1 = 0.9\omega_{rf}, \omega_1 = \omega_{rf}, \omega_1 = 1.1\omega_{rf}$) values passing Rabi resonance and MW attenuation below 200 mW. The results suggest that the spectrum detected at 35 dB (0.0636 mW) can be considered as the expected spectrum at Rabi resonance. Besides, it can be noted that while the spectrum at low $P_{MW} = 38$ dB exhibits fairly good agreement with the simulated spectrum at $\omega_1 = 0.9\omega_{rf}$, other two simulated spectra at higher $P_{MW} = 35$ dB and $P_{MW} = 34$ dB show clearly detectable deviation (broadening of the linewidth and lowering of spectral intensities) from the experimental spectra. Differences arise due to the inhomogeneous character of detected spectra since the spectral lineshapes are closer to Gaussian type as compared with the calculated spectra which involve only Lorentzian lineshapes. In order to improve description of these spectra one should consider more than one spectral component which contributes to the inhomogeneous spectrum exhibiting different effective T_1 or T_2. For example, the same inhomogeneous lineshape detected at 35 dB (Fig. 5b) can be better approximated by assuming $\omega_1 = \omega_{rf}$ and cumulative contribution of two homogeneous spectral components with the corresponding intensities $0.3I_{c1}$ and $0.7I_{c2}$ exhibiting relaxation times $T_1 = 2$ ms, $T_2 = 3.7$ μs and $T_1 = 20$ μs, $T_2 = 3.7$ μs (Fig. 6), respectively. This is in agreement with the previously detected maximum of the saturation signal [9] as well as DM-EPR signal [11] of inhomogeneous line of P1 centers in diamond crystal where two

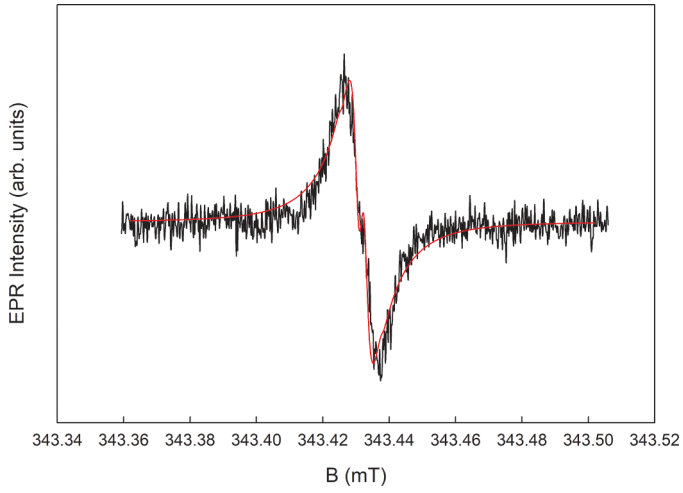

Figure 6. EPR spectra of P1 center detected at 35 dB of microwave power (solid black line) and corresponding simulated spectra (red line). Simulated line is composite and consists of two components $I = 0.3I_{c1} + 0.7I_{c2}$ with corresponding parameters for I_{c1} ($T_1 = 2$ ms, $T_2 = 3.7$ μs) and for I_{c2} ($T_1 = 20$ μs, $T_2 = 3.7$ μs).

components with effective relaxation times were introduced to better describe the inhomogeneous character of spectra.

However, in the present case it is more important to monitor the central part of the spectrum, which is more essential for the assignment of Rabi resonance, than the intensity itself and the outer part of the spectrum. For example, it is expected that ω_1 can be more accurately assigned in the experimental spectra in the close vicinity of ω_{rf} for the saturation region where $\omega_1 < \omega_{rf}$ than for the region where $\omega_1 > \omega_{rf}$ since the later one exhibits poor spectral information (only one singlet component) while the three spectral lines (two outer singlets of the same type and one singlet of the inversion type) are present in the former region. Moreover, in the saturation region where $\omega_1 < \omega_{rf}$ all spectral lines exhibit narrow character and features related to MS can be better resolved than in the saturation region where $\omega_1 > \omega_{rf}$. Thus, fairly good simulation can be achieved by employing expected relaxation times of the probe and the parameter value $\omega_1 = 0.9\omega_{rf}$ while the spectra in Fig. 5 (c) can provide more reliable assignment of B_1 than the spectra in the saturation region where ω_1 exceeds the frequency of Rabi resonance. Following above discussions, the spectrum measured at 35 dB (0.0636 mW) can be identified as spectrum at Rabi resonance and the value of $B_1 = 3.57$ μT correlated with the applied MW power. In the typical saturation measurements one varies B_1 by changing P_{MW} and conversion of P_{MW} into B_1 is determined by conversion efficiency constant C such that $B_1 = C(P_{MW})^{1/2}$, where P_{MW} is given in W units [6]. Since the C value is also characteristic constant of MW resonator (cavity), there is possibility to determine it from the known values of B_1 and P_{MW}. For instance, one obtains $C = 0.44$ mT/(W)$^{1/2}$ value for the Bruker ER 4118X-MD5 resonator which was employed in the above experiments. The obtained value is in good agreement with the expected value of 0.42 mT/(W)$^{1/2}$ for loaded Q-factor of 4000, as indicated in the Bruker product specification [23] for this type of resonators. Moreover, in order to test the present method for estimating B_1, the resonator conversion factor for different types of resonators was employed. The same sample was inserted in the Rectangular cavity TE_{102} ($C \sim 0.14$ mT/(W)$^{1/2}$, assuming Q-factor of 3500) [6, 24] which was used instead of Bruker ER 4118X-MD5 while all detection parameters were kept the same. Despite the lower signal to noise ratio obtained with the later resonator, the effect of Rabi resonance on P1 spectrum can be clearly assigned at significantly higher P_{MW} than the one required for the same effect of the former resonator. The spectrum detected in the vicinity of Rabi resonance ($\omega_1 < \omega_{rf}$) and the simulated spectrum calculated by employing following parameters: $\omega_1 = 0.9\omega_{rf}$, $T_1 = 2$ ms and $T_2 = 3.7$ μs are shown in Fig. 7. The experimental spectrum was recorded at $P_{MW} = 0.633$ mW while the smaller conversion factor was

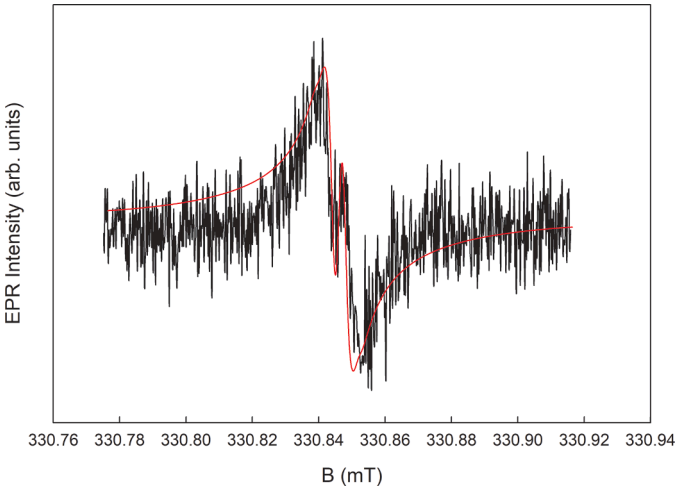

Figure 7. EPR detected spectra of P1 center acquired in the Rectangular cavity TE_{102} at $P_{MW} = 0.633$ mW (solid black line) and the corresponding simulated ones (red line). The simulated spectrum was calculated by employing following parameters $\omega_1 = 0.9\omega_{rf}$, $T_1 = 2$ ms and $T_2 = 3.7$ μs.

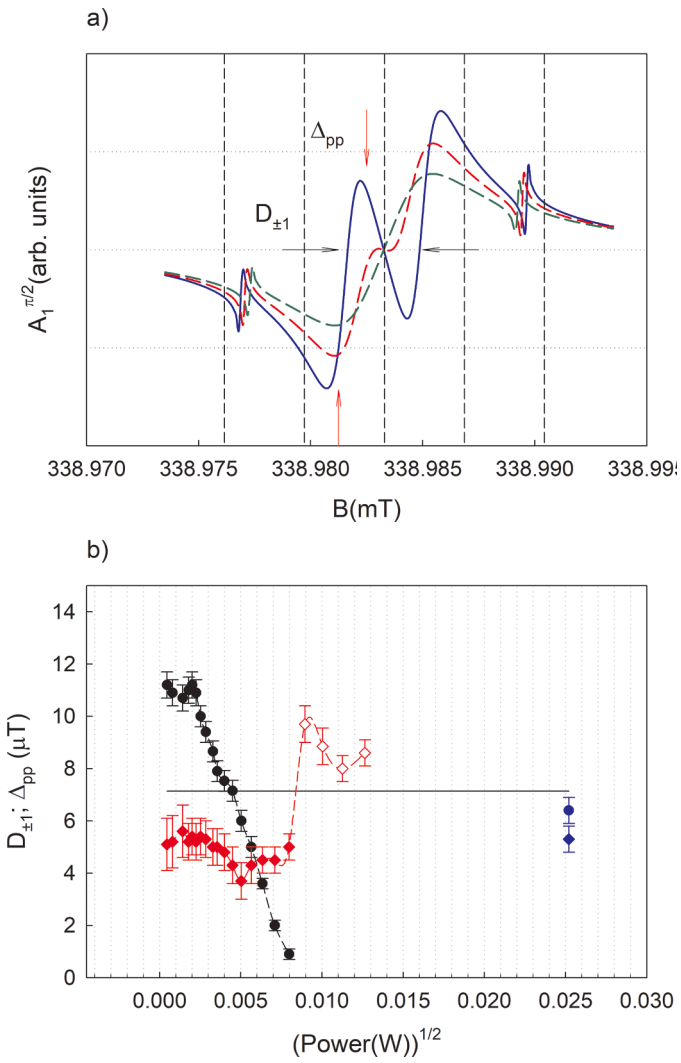

Figure 8. a). The first-harmonic out-of-phase absorption EPR signal calculated from Eq.2 as a function of ω_1 assuming $\omega_2 \ll \omega_1 \approx \omega_{rf}$: $\omega_1 = 0.9\omega_{rf}$(continuous line), $\omega_1 = \omega_{rf}$ (short-dashed line) and $\omega_1 = 1.1\omega_{rf}$ (long-dashed line). Parameter values are: $\omega_2/2\pi = 27$ kHz, $\omega_{rf}/2\pi = 100$ kHz, $T_1 = 2$ ms, $T_2 = 146$ μs. The vertical dashed lines denote positions for expected modulation sidebands at $\pm k\omega_{rf}$ for $k = 0,1,2$. Two horizontal arrows denote splitting distance defined as qualitative splitting parameter $D_{\pm1}$ while two orthogonal arrows denote qualitative parameter for peak-to-peak linewidth Δ_{pp}. b). Detected qualitative spectral parameters $D_{\pm1}$ (circles) and Δ_{pp} (diamond) as function of square root of microwave power. The full symbols correspond to low power region where both sidebands are present. Empty symbols correspond to high power region where only single line is present. Horizontal line denotes marker at $2\omega_{rf} \approx 7.14$ μT splitting between two first sidebands ($k = \pm1$) for the typical unsaturated modulation spectrum. Dotted lines connect experimental points. Experiments were performed using Bruker ER 4118x-MDS microwave cavity while two additional data (blue, full circles and diamond) at high region of microwave power were acquired using Rectangular cavity TE_{102}. In both experiments all recording parameters were kept the same, except the microwave power which was variable parameter.

expected than for the Bruker ER 4118X-MD5 cavity. It can be noted that the evaluated value of $C = 0.13$ mT/(W)$^{1/2}$ derived from the experimentally detected data nearly coincides with the predicted C value for the Rectangular cavity TE_{102}. Applied test on the two different resonators with corresponding conversions of MW power into B_1 supports above model for evaluating B_1 by employing CW-EPR out of phase spectra in the vicinity of the Rabi resonance.

5.2. Qualitative spectral parameters in the vicinity of Rabi resonance of the first harmonic out-of-phase experimental spectrum

In order to avoid complete simulation of the experimental spectra in the saturation regime in the vicinity of the Rabi resonance, it is convenient to introduce some qualitative spectral parameters which would reflect significant change in the monitored region. Moreover, these parameters should represent some effective properties related to MS spectrum. Under the condition of $\omega_2 > \omega_1 \ll \omega_{rf}$ typical first harmonic out-of-phase MS spectrum is characterized with the central line at $\Delta = 0$ and sidebands almost at $\Delta = k\omega_{rf}$ exhibiting components of dispersive shape and being anti-symmetric with respect to the central line [12]. Under the condition of "weak modulation near the Rabi resonance" this MS spectrum is changed and is described by relation (2) as presented in Fig. 8a. The most prominent changes can be summarized as broadening and shifting of spectral components, the phenomenon which depends on the sideband index k. In addition, different sideband components begin to overlap due to strong broadening. Thus, it can be noticed that the shape of each sideband $(k = \pm 1)$ consisting of two phonons, (k = -1, RF emission and MW absorption) and (k = +1, RF absorption and MW absorption) is changed towards absorption lineshape when ω_1 approaches Rabi resonance. At $\omega_1 > \omega_{rf}$, due to the broadening, these two sidebands form composite line, which is similar to the one broad dispersive line or to the derivative line usually detected in CW-EPR (Fig. 8a). The qualitative spectral parameter, which includes effects of broadening as well as transformation of the lineshape in the saturation region where $\omega_1 < \omega_{rf}$ can be related to the splitting $D_{\pm 1}$ between two shifted $(k = \pm 1)$ sidebands. The second qualitative spectral parameter can be related to the peak-to-peak linewidth Δ_{pp} of these sidebands with transformed lineshape. The arrows in Fig. 8a denote positions of these qualitative parameters in the simulated spectrum. It is expected that in the case of low saturation, under condition $\omega_2 > \omega_1 \ll \omega_{rf}$, values of $D_{\pm 1}$ approach distance between the first sidebands $(2\omega_{rf})$ while the value of Δ_{pp} approaches the value of peak-to-peak linewidth of the sideband $(\delta_{pp} = 1/\pi\sqrt{3}\,T_2)$. It is important to note that both suggested parameters exhibit significant changes at Rabi resonance, $D_{\pm 1}$ converge to zero value while Δ_{pp} to "discontinuity" (sharp increasing). Therefore, these properties can help in assignment of the spectrum at Rabi resonance within the series of detected CW-EPR spectra produced in saturation regime. This idea is presented in Fig. 8b showing $D_{\pm 1}$ and Δ_{pp} parameters as a function of MW saturation. It is useful to introduce the distance between two regular $k = \pm 1$ sidebands at $2\omega_{rf} \approx 7.14$ μT as a marker value. It can be expected that CW-EPR lineshape with the corresponding parameters detected in the region below the marker value of MS (Fig. 8b) produce noticeable effects while above this value their contribution become minor in comparison with the contribution of the other modulation and inhomogeneous line broadening effects. The obtained data clearly show convergence to zero value of $D_{\pm 1}$ and "discontinuity" for Δ_{pp} parameter at nearly the same MW power value. Thus, presented data support clear indication of MW power value at which the Rabi resonance is expected. Besides, by employing the optimal detection parameters of CW-EPR as discussed above, one detects a large variation of $D_{\pm 1}$ and Δ_{pp} values on the wide scale of MW power saturation. For example, $D_{\pm 1}$ exhibits a significant increase above the marker line in the limit of weak MW power. In order to explain such behavior and describe in this perspective the whole monitored MW power range, $D_{\pm 1}$ and Δ_{pp} parameters were calculated and correlated with experimental data while assuming $\omega_1 = \omega_{rf}$ resonance condition at 35 dB as discussed above. In addition, the variation of $D_{\pm 1}$ parameter for the three representative T_2 values ($T_2 = 14.6$ μs, $T_2 = 2.92$ μs, $T_2 = 1.46$ μs) and $T_1 = 2$ ms as a function of ω_{rf}/ω_1 is presented in Fig. 9a. Calculated parameters for the longest relaxation time shows the expected behavior approaching the marker value at low MW field and diverging to zero value at the very close vicinity of $\omega_{rf}/\omega_1 = 1$ (Rabi resonance). By gradually decreasing T_2 (increasing homogeneous linewidth), $D_{\pm 1}$ cross over the marker value and exhibit larger values than the marker in the limit of weak MW power. It can be noted that divergence toward zero value is shifted from the value of $\omega_{rf}/\omega_1 = 1$ to larger values of $\omega_{rf}/\omega_1 \sim 1.05$ at normalized MW power scale. The most of experimental values of $D_{\pm 1}$ values coincide with the calculated $D_{\pm 1}$ in the close interval around 1 at normalized MW power scale while supporting appearance of Rabi resonance within this narrow interval. The deviation of the experimental data from the calculated $D_{\pm 1}$ for presented homogeneous line at low MW power indicates that the experimental $D_{\pm 1}$ values can be explained as an average contribution due to the composite inhomogeneous line. The same values of the relaxation times were used in the calculation of Δ_{pp} parameters (Fig. 9b) and all the data show "discontinuity" in the vicinity of 1 at normalized MW power axis. It can be noticed that the values of Δ_{pp} for the shortest relaxation time exceed the marker value. This phenomenon is a consequence of the homogeneous linewidth which becomes larger than the splitting between the sidebands ($\delta > \omega_{rf} 2\pi$) while MS effects on such broad line are smaller than on the narrow spectral line ($\delta < \omega_{rf} 2\pi$). The simulation of Δ_{pp} for the broadest homogenous line also shows the largest shift of 'discontinuity' (larger value than 1) in comparison to narrower homogeneous lines (longer relaxation times). The average of experimental data in Fig. 9b can be described with calculated Δ_{pp} for $T_2 = 2.92$ μs. The obtained value shows a good agreement with effective T_2^* within the

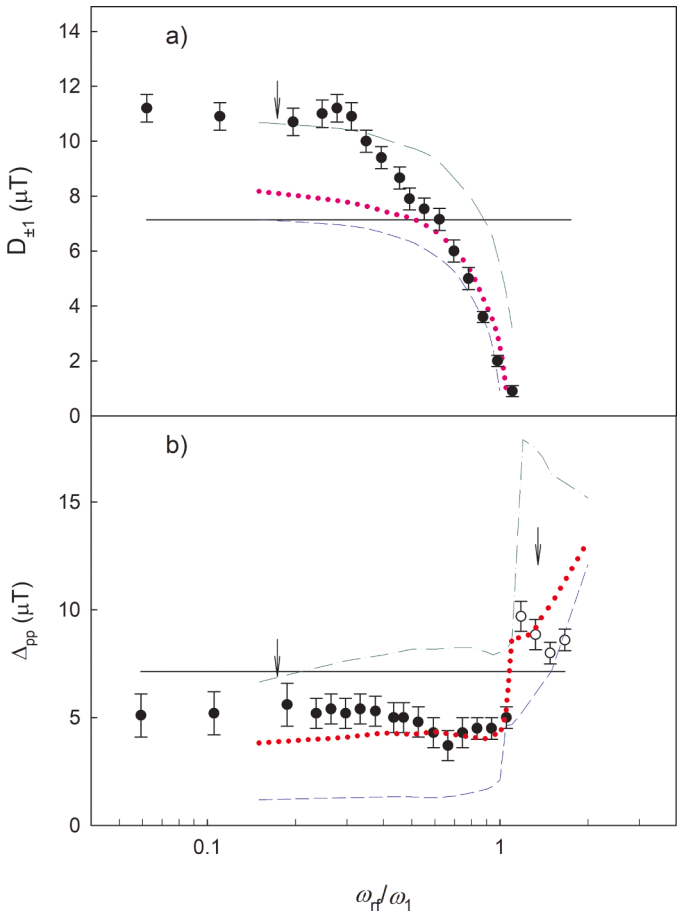

Figure 9. Calculated qualitative spectral parameters $D_{\pm 1}$ (a) and Δ_{pp} (b) as function of ω_1/ω_{rf} by employing eq. 2 and parameters $T_2 = 14.6$ μs, (short dashed line, blue) $T_2 = 2.92$ μs (dotted line, red) and $T_2 = 1.46$ μs (long dashed line, green). The experimental data described in Fig. 9. were correlated with calculated data by assuming that the last experimental point (full circles and diamonds) coincides with 1 at abscissa axis. The arrows denote expected position of qualitative spectral parameter values detected in ref.22.

interval of 3.7- 5.9 μs. The effective T_2* originates from dipole-dipole coupling between P1 centers as was estimated for this ([N_s^0] <1ppm) crystal from DEER technique [10]. It is important to realize that the expected minimum in $D_{\pm1}$ or "discontinuity" of Δ_{pp} shows relatively small shift from 1 (from 1 to ~1.05) apart from the fact that T_2 was changed more than one order of magnitude. Thus, correlation between the lowest $D_{\pm1}$ value and the last point of Δ_{pp} value before "discontinuity" with 1 at abscisa axis leads to the relatively good approximation (~5%) of the estimated Rabi resonance. It can be seen (Fig. 8b) that one can estimate both qualitative parameters from the spectra detected using Rectangular cavity TE_{102} also below $2\omega_{rf}$ marker. Generally, the above consideration indicates that, if the employed HPHT diamond standard exhibits Δ_{pp} and $D_{\pm1}$ below $2\omega_{rf}$ value in the vicinity of Rabi resonance, one can expect relative high accuracy (within 10%) in the estimation of B_1. In the case when the qualitative parameters have significantly larger values than the $2\omega_{rf}$ value, the above model is not appropriate and correct assignment of resonance condition for such spectra is not reliable. A good example for such behavior can be seen in detected and calculated out of phase CW-EPR spectra for TEMPONE sample in 90 % glycerol at 20°C acquired at $\omega_{rf}/2\pi = 100$ kHz with corresponding relaxation times $T_1 = 2.2$ μs and $T_2 = 0.06$ μs [25]. Theoretical model which was used to describe these absorption signal detected at first harmonic out-of-phase with respect to the field modulation was based on Bloch equations that include the microwave and the Zeeman modulation field [26, 27]. The approximate solution obtained by iterative solution of Bloch equations was applied for the simulation of spectra as a function of H_1 (Fig. 1 in ref. 25) and exhibits the lineshape profile quite similar to the one seen for diamond sample. However, the coalescence of two lines (as expected at Rabi resonance) can be seen at significantly higher $H_1 \sim 0.055$ G than it was expected for $\omega_{rf}/2\pi = 100$ kHz in the above simulation. Moreover, it is easy to note from the experimental spectra that approximate values of corresponding Δ_{pp} and $D_{\pm1}$ (~ 0.1 mT) parameters are significantly above $2\omega_{rf}$ (7.14 μT) threshold value for the employed modulation frequency.

Regarding the out-of-phase spectrum for diamond crystal with low density of nitrogen impurity reported previously [22] it was suggested that its detail description can be better achieved in the frame of the present model [12] than the earlier applied model of modified Bloch equation [27]. Indeed, Fig. 2 from the reference [22] shows microwave power dependence of CW-EPR spectra quite similar to the one presented in Figs. 4 and 5. by employing similar spectroscopic parameters. Since, the complete data information for the reported lineshapes are not available, the qualitative parameters of these spectra were used for the present analyses. The value of parameter $D_{\pm1} = 11$ μT was explicitly given for spectra recorded at 25 dB ($B_1 = (30 \pm 5)$ μT at 0 dB) and it is expected to approach zero value at ≤ 17 dB. The value of qualitative parameter $\Delta_{pp} \approx 6.5$ μT was estimated. Both parameters are included in Fig. 10 (as arrows) by assuming that resonance is detected at 17 dB and difference between points at dB scale is correlated with the position at normalized abscisa scale. The position of this points approximately coincides with the presented experimental data which are described with the corresponding lineshape parameters ($T_1 = 2$ ms, $T_2 = 1.46$ μs,). It can be noticed that these parameter values are close to parameters used in the applied spectral model calculation ($T_1 = (2.7 \pm 1.2)$ ms, $T_2 = (0.87 \pm 0.05)$ μs) while derived $B_1 \sim 4.2$ μT at 17 dB differs 20% from the value $B_1 \sim 3.6$ μT expected at the resonance condition. In order to check the model for spectral lineshape description (previously suggested in ref. 22), significantly larger parameter $D_{\pm1} = 21$ μT at 25 dB was calculated as compared with the experimental $D_{\pm1} = 11$ μT value [22]. Therefore, according to the present analyses no significant discrepancy between the calculated and experimentally obtained $D_{\pm1}$ parameter and B_1 value at resonance condition can be concluded (Fig. 9). Since these parameters were found almost within the experimental error estimated in the previous study [22], the presented MS model shows capability to successfully describe appearance of multicomponent spectrum of P1 center detected at first harmonic as a function of microwave power.

It is also important to note that the same standard for B_1 estimation will be operative at lower temperatures where one expects significant increase of T_1 for the P1 center in HPHT diamond crystal [9]. This is demonstrated by spectral simulation (Fig. 2) showing larger spectral intensity and better resolution of the effect of Rabi resonance.

5. Conclusion

In the present consideration basic methodology with theoretical background was described how to employ commercial HPHT diamond crystal as a standard for detecting MW field intensity by applying ordinary CW-EPR spectroscopy.

The suggested model keeps all advantages from the saturation model discussed in detail for HTPH diamond except for the *S/N* ratio, which is smaller than in the saturation model due to the low concentration of P1 center. However, there are several possibilities which can improve sensitivity of the presented method. The sensitivity and *S/N* ratio can be additionally improved by applying optimization of recording parameters for the critical spectrum such as the increase of the number of accumulated spectra in comparison to the present work where most of the spectra were recorded by applying only one or three number of scans (Fig. 7). Additionally, the samples with larger concentration of P1 centers, which exhibit broader δ_{pp}^I, can be used by applying higher modulation RF ($> \omega_{rf}/2\pi = 100$ kHz) and, thus, larger distance between the sidebands can be achieved leading to the larger impact of MS on the spectrum near the Rabi resonance. For such improvement one needs to employ the Lock-In amplifier with ability to work at higher frequencies. It is also important to stress, that small dimension of diamond crystal together with very stable concentration of P1 centers makes this probe very convenient in manipulation within the cavity and in recording the EPR signal compared with other samples. For DNP enhanced NMR it is important that one can assigned lower value of B_1 in the comparison to the saturation model.

Declaration of Competing Interest

The authors declare that they have no known competing financial interests or personal relationships that could have appeared to influence the work reported in this paper.

Acknowledgment

This work was fully supported by the Croatian Science Foundation under the project number IP-2018-01-3168. The authors highly acknowledge the diamond samples obtained from Susumu Takahashi and Ivan Hrvoić.

References

[1] E.L. Ginzton, Microwave measurements, McGraw-Hill, New York, 1957.
[2] J.H. Freed, D.S. Leniart, J.S. Hyde, Theory of Saturation and Double Resonance Effects in ESR Spectra. III. rf Coherence and Line Shapes, The Journal of Chemical Physics 47 (1967) 2762–2773.
[3] D.P. Dalal, S.S. Eaton, G.R. Eaton, The effects of lossy solvents on quantitative EPR studies, Journal of Magnetic Resonance 44 (1981) (1969) 415–428.
[4] M.A. Hemminga, F.A.M. Leermakers, P.A. de Jager, Quantitative measurement of B1 in ESR and saturation-transfer ESR spectroscopy, Journal of Magnetic Resonance 59 (1984) (1969) 137–140.
[5] A.I. Vistnes, L.R. Dalton, Experimental methods to determine the microwave field strength in electron spin resonance, Journal of Magnetic Resonance 54 (1983) (1969) 78–88.
[6] G.R. Eaton, S.S. Eaton, D.P. Barr, R.T. Weber, Quantitative EPR, Springer Vienna, 2010.
[7] M. Peric, B. Rakvin, A. Dulcic, Measurement of Microwave Field-Strength in Electron-Spin-Resonance by a Pulsed Modulation Technique, Journal of Magnetic Resonance 65 (1985) 215–221.
[8] B. Rakvin, D. Carić, M. Kveder, Enhanced accuracy of the microwave field strength measurement in a CW-EPR by pulsed modulation technique, Journal of Magnetic Resonance 287 (2018) 123–127.

[9] A.M. Carroll, S. Eaton, G. Eaton, K.W. Zilm, Electron spin relaxation of P1 centers in synthetic diamonds with potential as B1 standards for DNP enhanced NMR, Journal of Magnetic Resonance 322 (2021), 106875.
[10] V. Stepanov, S. Takahashi, Determination of nitrogen spin concentration in diamond using double electron-electron resonance, Physical Review B 94 (2016), 024421.
[11] B. Rakvin, D. Carić, M. Kveder, Detection of narrow lines in the inhomogeneously broadened line of P1 centers in diamond by double modulation EPR spectroscopy, Appl Phys Lett 117 (2020), 153503.
[12] A.P. Saiko, R. Fedaruk, S.A. Markevich, Multi-photon transitions and Rabi resonance in continuous wave EPR, Journal of Magnetic Resonance 259 (2015) 47–55.
[13] M. Kalin, I. Gromov, A. Schweiger, The continuous wave electron paramagnetic resonance experiment revisited, Journal of Magnetic Resonance 160 (2003) 166–182.
[14] M. Kälin, M. Fedin, I. Gromov, A. Schweiger, Multiple-Photon Transitions in EPR Spectroscopy, in: J. Dolinšek, M. Vilfan, S. Žumer (Eds.), Novel NMR and EPR techniques, Springer Berlin Heidelberg, Berlin, Heidelberg, 2006, pp. 143–183.
[15] J.H.N. Loubser, J.A.v. Wyk, Electron spin resonance in the study of diamond, Reports on Progress in Physics 41 (1978) 1201–1248.
[16] J.A.v. Wyk, E.C. Reynhardt, G.L. High, I. Kiflawi, The dependences of ESR line widths and spin - spin relaxation times of single nitrogen defects on the concentration of nitrogen defects in diamond, Journal of Physics D: Applied Physics 30 (1997) 1790–1793.
[17] A. Cox, M.E. Newton, J.M. Baker, 13C,14N and15N ENDOR measurements on the single substitutional nitrogen centre (P1) in diamond, Journal of Physics: Condensed Matter 6 (1994) 551–563.
[18] S. Zhang, S.C. Ke, M.E. Zvanut, H.T. Tohver, Y.K. Vohra, g tensor for substitutional nitrogen in diamond, Physical Review B 49 (1994) 15392–15395.
[19] A.M. Portis, Rapid Passage Effects in Electron Spin Resonance, Phys Rev 100 (1955) 1219–1221.
[20] M. Weger, Passage effects in paramagnetic resonance experiments, The Bell System Technical Journal 39 (1960) 1013–1112.
[21] D.G. Mitchell, M. Tseitlin, R.W. Quine, V. Meyer, M.E. Newton, A. Schnegg, B. George, S.S. Eaton, G.R. Eaton, X-band rapid-scan EPR of samples with long electron spin relaxation times: a comparison of continuous wave, pulse and rapid-scan EPR, Mol Phys 111 (2013) 2664–2673.
[22] R.C. Barklie, J. Guven, 13C hyperfine structure and relaxation times of the P1 centre in diamond, Journal of Physics C: Solid State Physics 14 (1981) 3621–3631.
[23] J. Möser, K. Lips, M. Tseytlin, G.R. Eaton, S.S. Eaton, A. Schnegg, Using rapid-scan EPR to improve the detection limit of quantitative EPR by more than one order of magnitude, Journal of magnetic resonance (San Diego, Calif.: 1997) 281 (2017) 17–25.
[24] B.L. Bales, L. Kevan, Electron paramagnetic resonance studies of silver atom formation and enhancement by fluoride ions in .gamma.-irradiated frozen silver nitrate solutions, The Journal of Physical Chemistry 74 (1970) 1098–1103.
[25] V.A. Livshits, T. Páli, D. Marsh, Spin Relaxation Measurements Using First-Harmonic Out-of-Phase Absorption EPR Signals, Journal of Magnetic Resonance 134 (1998) 113–123.
[26] T. Páli, V.A. Livshits, D. Marsh, Dependence of Saturation-Transfer EPR Intensities on Spin–Lattice Relaxation, Journal of Magnetic Resonance, Series B 113 (1996) 151–159.
[27] K. Halbach, Uber eine neue Methode zur Messung von Relaxationszeiten und über den Spin von Cr53, Helv. Phys. Acta 27 (1954) 259–282.